Performance Evaluation on FPGA-Implemented UWB-IR Receiver for In-Body to Out-of-Body Communication Systems

Yuto Shimizu[1], Daisuke Anzai[1] and Jianqing Wang[1]

Abstract— **In order to design an optimized transceiver structure of ultra wideband (UWB) transmission in in-body to out-of-body communications, it is necessary to make the transceiver structure be easily adjustable in order to realize a good communication performance in an experimental environment. For this purpose, we first implement our develop UWB-impulse radio (IR) receiver structure for the in-body to out-of-body communication in a field programmable gate array (FPGA) board, and evaluate the fundamental communication performance of the FPGA-implemented UWB-IR receiver by a biological-equivalent liquid phantom experiment. The FPGA configuration results indicate that our FPGA realization of the UWB-IR receiver has accomplished good communication performance with few FPGA slices. Moreover, the evaluation results in the liquid phantom experiment show that the FPGA-implemented UWB-IR receiver can achieve a bit error rate (BER) of 10^{-3} up to a communication distance of 70 mm with ensuring a high data rate of 2 Mbps.**

I. Introduction

Wireless body area networks (BANs) are attracting much attention as a promising technology in health care and medical applications [1]–[3]. The in-body to out-of-body communication plays an important role in wireless BANs because it can transmit various vital signals and image/video data from the inside of human body to the outside medical equipment [4], [5]. Some typical applications include wireless cardiac pacemaker and wireless capsule endoscope. The former requires a highly reliable communication performance for vital signal monitoring, and the latter requires a higher data rate for real-time image transmission.

To realize the implant communications, the 400 MHz band and 2.4 GHz band are usually chosen. For example, a commercially available implant communication chip for cardiac pacemaker employs the 400 MHz band for data transmission and the 2.4 GHz band for waking-up and control [6]. The literatures [7], [8] have reported that all of wireless capsule endoscope techniques employ 400 MHz, 2.4 GHz or dozens of MHz band with narrow-band modulation schemes, such as frequency shift keying (FSK) or binary phase shift keying (BPSK). The data rate is limited to several hundred kbps. However, for the implant communication application, a wireless capsule endoscopy system, for instance, requires a higher data rate in order to realize a real-time image and video transmission.

In order to fulfill the above requirements, this paper pays attention to ultra wideband (UWB) transmission. As UWB transmission schemes, UWB-impulse radio (UWB-IR), direct sequence-UWB (DS-UWB), and multiband-orthogonal frequency division multiplexing (multiband-OFDM) have been proposed [9]–[11]. Of the all UWB schemes, UWB-IR is a technique that iteratively transmits extremely short pulses on the nanosecond time duration per bit. Therefore, it has a merit in respect of low power consumption. For low complexity and low power consumption in the UWB-IR communication system, non-coherent detection, namely, energy detection is better choice than coherent detection because the energy detection does not require a high frequency synthesis, so that, radio frequency (RF) front-end can be significantly simplified, and the analog to digital conversion speed can be reduced to the symbol rate scale.

However, in implant BANs, the UWB-IR signals suffer from large attenuation, which may lead to undesired performance degradation. Therefore, it is important to develop a reliable transmission system and investigate the transmission performance of real implant BANs. In our previous work, the UWB-IR transmission performance was actually evaluated via a living animal experiment. However, the UWB-IR receiver was realized in a computer and the implementation aspect of the UWB-IR receiver side was rarely discussed [12]. Therefore, this paper aims to implementation of the UWB-IR receiver structure into a field programmable gate array (FPGA) board, and furhermore, we evaluate the performance of our FPGA-implemented UWB-IR receiver by a biological-equivalent liquid phantom experiment.

The remainder of this paper is organized as follows. Section II presents the design of the developed UWB-IR communication system including the design of FPGA configuration. Section III describes the communication performance of the implemented UWB-IR receiver by a biological-equivalent liquid phantom experiment. Finally, Section IV concludes this paper.

II. FPGA Implementation of UWB-IR Receiver Structure

A. Receiver Design

In this paper, we implement the UWB-IR receiver structure into an FPGA board. As for the transmitter structure, we employed a multi pulse postion modulation (MPPM) scheme (for details refer to [12]).

In our previous study [13], we have found that the power delay profile can be well represented as a two-path model with a very small mean time interval in the order of nano seconds. This means that the multipaths are almost indistinguishable in the received signal and the multipath fading

[1]Graduate School of Engineering, Nagoya Institute of Technology Gokiso-cho, Showa-ku, Nagoya, Aichi 466-8555, Japan anzai@nitech.ac.jp and wang@nitech.ac.jp

978-1-4244-7929-0/14/$26.00 ©2014 IEEE

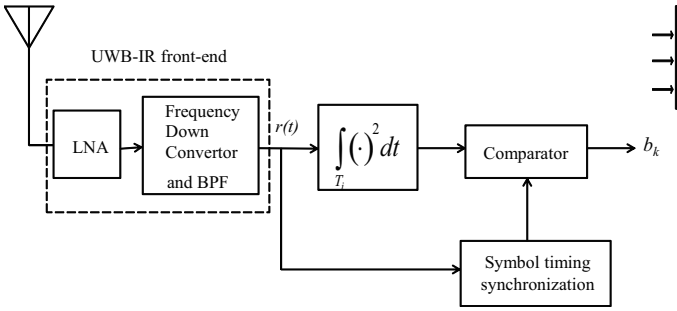

Fig. 1. Receiver structure

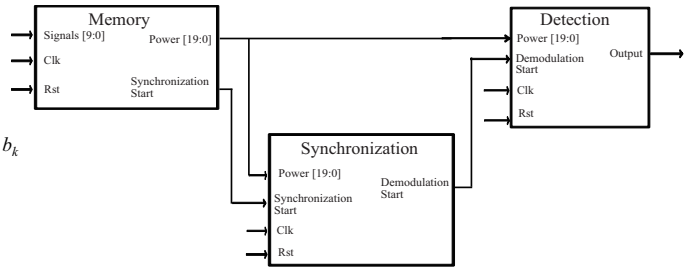

Fig. 2. Overview of FPGA configuration

effect is not dominative. So in this study we try to investigate the communication performance without channel estimation to confirm whether our proposed UWB transmission system can work well in a real living body environment. As mentioned previously, we pay attention to the energy detection as the receive detection scheme. In the energy detection, since the binary MPPM chooses one from two location assignments in the k-th symbol, we calculate two kinds of k-th energies for the corresponding pulse locations. Fig. 1 shows the receiver structure of the UWB-IR communication.

As for the FPGA implementation, Fig. 2 shows the overview of the FPGA configuration for UWB-IR receiver. The developed UWB-IR receiver mainly consists of includes three components, such as a memory module, a synchronization module and a detection module. The memory module successively receives signals from the front-end of the receiver. Then, the received signals are transformed into squared values to calculate the energy of the received signal and stored in shift registers. The memory module stores the received signals for two symbol duration, and the stored data are sent to the synchronization and detection modules at a proper timing.

In order to accurately detect the UWB pulse position, it is necessary to perform symbol timing synchronization. So, the synchronization module estimates the symbol timing by using the received UWB-IR signals. In the symbol timing synchronization, the timing is estimated based on the cross-correlation between the received signal $r(t)$ and the pulse detection intervals $s(t)$ as

$$\hat{\tau}_{timing} = \arg\max_{\tau} \int_0^{N^{pre}T_s} r(t)s(t-\tau)dt \qquad (1)$$

where N^{pre} indicates the number of UWB pulses for the preamble header. In (1), $\arg\max(\cdot)$ stands for the argument of the maximum of $(\cdot)$. Here, the preamble header is composed of 16 symbols selected from a pseudo random (PN) sequence (namely, we set N^{pre} to 16). Fig. 3 shows the flowchart of the symbol timing synchronization.

Finally, we explain the principle of the detection module. From Fig. 1, we perform the energy detection to demodulate the received signals. The detection module makes use of the symbol timing from the synchronization module. In the energy detection, since the binary MPPM chooses one from two location assignments in the k-th symbol, we calculate two kinds of k-th energies for the corresponding pulse locations from the received signal $r(t)$ as follows:

$$E_0^k = \sum_{l=1}^{L} b_0^l \int_{(k-1)T_s+(l-1)T_c}^{(k-1)T_s+(l-1)T_c+T_d} [r(t)]^2 dt \qquad (2)$$

$$E_1^k = \sum_{l=1}^{L} b_1^l \int_{(k-1)T_s+(l-1)T_c}^{(k-1)T_s+(l-1)T_c+T_d} [r(t)]^2 dt \qquad (3)$$

where T_d denotes the integration time. Note that T_d is much smaller than the symbol duration T_s and the chip slot duration T_c in UWB-IR transmission. Comparing E_0^k and E_1^k, the received bit information $\hat{b}_k$ can be decided as

$$\hat{b}_k = \begin{cases} 0 & \text{if } E_0^k > E_1^k \\ 1 & \text{otherwise.} \end{cases} \qquad (4)$$

We note that as can be seen from the above equation, the MPPM requires no threshold.

TABLE I
FPGA CONFIGURATION RESULTS

Slices	Available	Used
Registers	301440	10049 (3%)
LUTs (LookUp Tables)	150720	17918 (11%)
LUT-FF-pairs	77794	2711 (10%)
IOB	600	71 (11%)
BUF	32	2 (6%)
DSP48E1	768	1 (0.1%)

B. Result of FPGA Configuration

The circuit design of the UWB-IR receiver structure was developed in Verilog-HDL language, and the developed circuit was configured on Xilinx Virtex-6 FPGA board (XC6VLX204T-1FFG1156FPGA). Table I shows the results of the FPGA configuration. As can be seen from Table I, our FPGA realization of the UWB-IR receiver requires quite few FPGA slices. The reason is that we employed the UWB-IR transmission and the energy detection as a detection scheme of the UWB-IR signals, so that, the circuit of the receiver needs no oscillator circuit for carrier regeneration and no template signal generator for correlation detection.

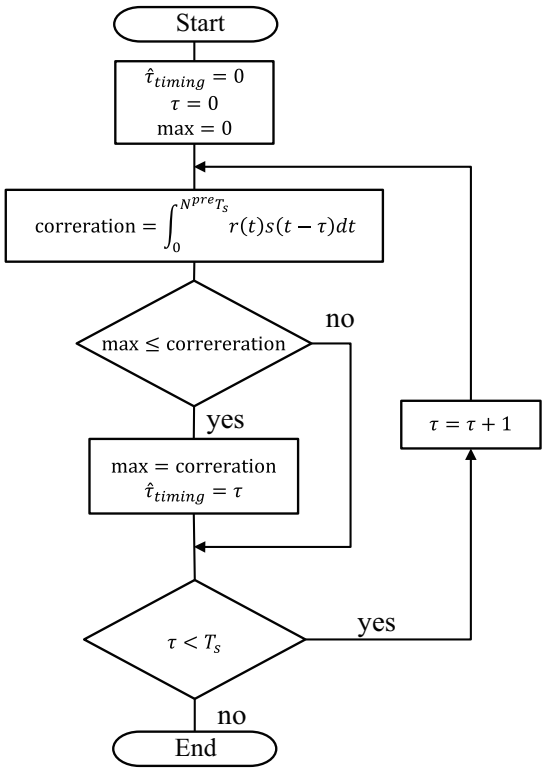

Fig. 3. Flowchart of the symbol timing synchronization

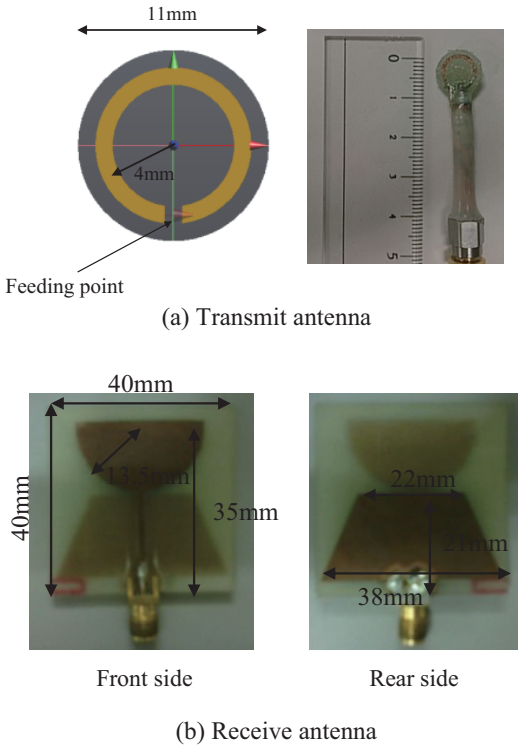

Fig. 4. Transmit and receive antennas

TABLE II
UWB-IR TRANSCEIVER PARAMETERS

Average transmitted power spectrum density	-47 dBm/MHz
Peak transmitted power	-25 dBm
Pulse width τ	100 psec
Bandwidth after front-end processing	700 MHz
Chip time T_c	62.5 nsec
Bit rate	8 Mbps ($L = 2$) 2 Mbps ($L = 8$)
Forward error correction	None
Length of pilot signal	16 symbols

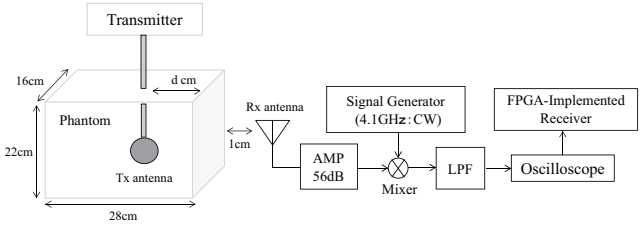

Fig. 5. Phantom experiment setup.

III. Performance Evaluation Experiment with Liquid Phantom

Here, let us perform experiments for evaluation of the fundamental performance of the implemented UWB-IR receiver. For this purpose, we measured the fundamental characteristics of the UWB-IR transceivers in a liquid phantom simulating a human body. In this experiment, we used a planar unbalance dipole antenna as an on-body receive antenna put on the liquid phantom surface with a spacing of 1 cm. For the in-body transmit antenna, we employed a planer loop antenna, which is designed for 3.4-4.8 GHz UWB low-band wireless capsule endoscope. The both receive and transmit antennas are shown in Fig. 4 (for the detailed transmit/receive antenna characteristics, see [14]). The transmitter used in this experiment was produced by GIT Japan Inc.

Figs. 5 and 6 show the measurement setup with the liquid phantom and a picture of the phantom experiment, respectively. We used a vessel made from plastic material as the container in the liquid phantom experiment. We have checked the dielectric properties of the vessel and found that its loss is almost ignorable. The relative permittivity and conductivity of the liquid phantom at 4.1GHz, the center frequency of UWB low-band, were 36.1 and 3.4[S/m] respectively.

The transmit and receive antennas were connected to the transmitter and receiver with coaxial cables, respectively, and the two coaxial cables were arranged at right angle to each other for removing possible direct coupling between them.

In this experiment, we evaluated bit error rate (BER) performance for the FPGA-implemented UWB-IR receiver. The transmitter sent $10,000$ bits, and then we calculated the BER from comparison between the transmitted bit sequence and the received bit sequence. As for the symbol timing synchronization, we set length of pilot signals to 16 symbols. Moreover, we have also determined the optimal integration time T_d before conducting the experiment. The parameters of the UWB-IR transceivers are summarized in Table II. Fig. 7 shows the average BER performances for the

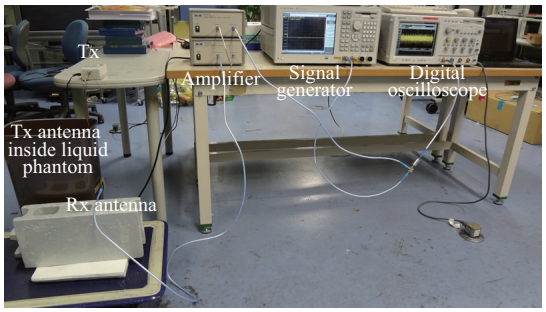

Fig. 6. View of phantom experiment.

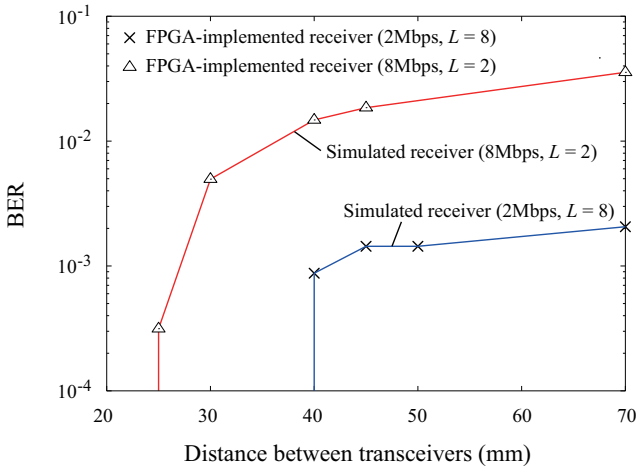

Fig. 7. BER performance for FPGA-implemented receiver.

FPGA-implemented UWB-IR receiver against the transceiver distance. For comparison purpose, Fig. 7 also includes the results for a simulated receiver developed in C language. Note that the FPGA-implemented receiver performs only fixed-point calculation, whereas the simulated receiver can deals with floating-point calculation. However, we can see from Fig. 7 that the difference between the both receivers is significantly small, so it is concluded that our FPGA implementation of the UWB-IR receiver has been successfully realized without any sacrifice of performance degradation.

Furthermore, as seen from Fig. 7, the BER performance is improved as the data rate decreases (namely, L increases). This is because we can accomplish higher E_b/N_0 after demodulation in the receiver as we set to lower value of L. Note that the BER performance of 10^{-2} is accomplished at the distance of around 70 mm when $L = 8$ (namely, the data rate is 2 Mbps). The achievement of the BER performance of around 10^{-2} to 10^{-3} means that it is possible to obtain an error-free BER ($< 10^{-10}$) if we adapt an adequate forward error correction code. This error-free BER satisfies the requirement for almost all implant BAN applications. Therefore, the FPGA-implemented UWB-IR receiver can establish a reliable communication link at the maximum distance of 70 mm in the biological-equivalent liquid phantom.

IV. Conclusions

This study has implemented our previously developed UWB-IR receiver structure in an FPGA board, and has evaluated the fundamental performance for the FPGA-implemented UWB-IR receiver by a liquid phantom experiment. The result of the FPGA configuration indicates that our FPGA realization of the UWB-IR receiver has accomplished good BER performance with few FPGA slices. Additionally, the FPGA-implemented receiver can achieve a BER performance of 10^{-3} up to a communication distance of 70 mm with ensuring a high data rate of 2 Mbps. Such an FPGA-implemented receiver provides a significant convenience for optimizing the receiver structure in an experimental environment. In view of our previous living animal experiment result, there is a sufficient potential to reach a data rate up to 8-10 Mbps with UWB-IR technique. This data rate should be able to provide a real-time image transmission for capsule endoscope application. Our future subject is to further improve the transceiver performance by optimizing the receiver structure with the FPGA implementation to increase the data rate and enlarge the in-body to out-of-body communication distance.

References

[1] H.B. Li and R. Kohno, "Body Area Network and Its Standardization at IEEE 802.15. BAN," *Advances in Mobile and Wireless Communications,* pp. 223–238, Springer, 2008.

[2] E. Monton, J.F. Hernandez, J.M. Blasco, T. Herve, J. Micallef, I. Grech, A. Brincat, and V. Traver, "Body area network for wireless patient monitoring," *IET Communications*, vol. 2, no. 2, pp. 215–222, Feb. 2008.

[3] J. Wang and Q. Wang, *Body Area Communications,* Wiley – IEEE, 2013.

[4] G. Iddan, G. Meron, A. Glukhovsky, and P. Swain, "Wireless capsule endoscopy," *Nature,* vol. 405, p. 417, May 2000.

[5] G. Costamagna, S.K. Shah, M.E. Riccioni, F. Foschia, M. Mutignani, V. Perri, A. Vecchioli, M.G. Brizi, A. Picciocchi, and P. Marano, "A prospective trial comparing small bowel radiographs and video capsule endoscopy for suspected small bowel disease," *Gastroenterology*, vol. 123, no. 4, pp. 999–1005, Oct. 2002.

[6] Zarlink Semiconductor Inc. URL: www.ZARLINK.com

[7] M.R. Yuce, and T. Dissanayake, "Easy-to-swallow wireless telemetry," *IEEE Microwave magazine.*, vol. 13, no. 6, pp. 90 – 101, Sept. 2012.

[8] M.R. Yuce, T. Dissanayake, and H.C. Keong, "Wireless telemetry for electronic pill technology," *IEEE Sensors*, pp. 1433–1438, Oct. 2009.

[9] M. Z. Win and R. A. Scholtz, "Ultra-wide bandwidth time-hopping spread spectrum impulse radio for wireless multiple-access communications," *IEEE Trans. Commun.,* vol. 48, pp. 679–691, Apr. 2000.

[10] P. Runkle, J. McCorkle, T. Miller, and M. Welborn, "DS-CDMA: The modulation technology of choice for UWB communications," in *Proc. IEEE Conf. on UWBST'03*, in CD-ROM, Nov. 2003.

[11] J. Balakrishnan, A. Batra, and A. Dabak, "A multi-band OFDM system for UWB communication," in *Proc. IEEE Conf. on UWBST'03*, in CD-ROM, Nov. 2003.

[12] D. Anzai, K. Katsu, R. Chavez-Santiago, Q. Wang, D. Plettemeier, J. Wang, and I. Balasingham, "Experimental evaluation of implant UWB-IR transmission with living animal for body area networks," *IEEE Trans. Microwave Theory Tech.*, vol. 62, no. 1, pp. 183–192, Jan. 2014.

[13] J. Shi, D. Anzai and J. Wang, "Channel modeling and performance analysis of diversity reception for implant UWB wireless link", *IEICE Trans. Commun.*, vol.E95-B, no.10, pp.3197-3205, Oct. 2012.

[14] Y. Morimoto, D. Anzai, and J. Wang, "Design of ultra wide-band low-band implant antennas for capsule endoscope application," in Proc. *7th International Symposium on Medical Information and Communication Technology (ISMICT)*, pp. 61–65, Tokyo, Japan, Mar. 2013.